

# Learning a Category-level Object Pose Estimator without Pose Annotations

Fengrui Tian<sup>1</sup>, Yaoyao Liu<sup>2</sup>, Adam Kortylewski<sup>4,5</sup>, Yueqi Duan<sup>3</sup>, Shaoyi Du<sup>1</sup>, Alan Yuille<sup>2</sup> and Angtian Wang<sup>2</sup>

<sup>1</sup>Xi'an Jiaotong University <sup>2</sup>Johns Hopkins University <sup>3</sup>Tsinghua University

<sup>4</sup>University of Freiburg <sup>5</sup>Max Planck Institute for Informatics

tianfr@stu.xjtu.edu.cn {yliu538, ayuille1, angtianwang}@jhu.edu

kortylew@cs.uni-freiburg.de duanyueqi@tsinghua.edu.cn dushaoyi@xjtu.edu.cn

## Abstract

3D object pose estimation is a challenging task. Previous works always require thousands of object images with annotated poses for learning the 3D pose correspondence, which is laborious and time-consuming for labeling. In this paper, we propose to learn a category-level 3D object pose estimator without pose annotations. Instead of using manually annotated images, we leverage diffusion models (*e.g.*, Zero-1-to-3) to generate a set of images under controlled pose differences and propose to learn our object pose estimator with those images. Directly using the original diffusion model leads to images with noisy poses and artifacts. To tackle this issue, firstly, we exploit an image encoder, which is learned from a specially designed contrastive pose learning, to filter the unreasonable details and extract image feature maps. Additionally, we propose a novel learning strategy that allows the model to learn object poses from those generated image sets without knowing the alignment of their canonical poses. Experimental results show that our method has the capability of category-level object pose estimation from a single shot setting (as pose definition), while significantly outperforming other state-of-the-art methods on the few-shot category-level object pose estimation benchmarks.

## 1 Introduction

The 3DoF rotation of objects is an inherent characteristic of real-world objects. Estimation of 3D poses of objects offers advantages for downstream applications, such as autonomous driving and robotics. Recent researchers [Wang *et al.*, 2021b; Wang *et al.*, 2021a; Yin *et al.*, 2022] tried to build category-level estimators to estimate object poses from a particular category. One popular solution is following the *Analysis-by-Synthesis* principle. Specifically, given a set of object images with annotated poses, these methods first build a 3D neural mesh as the category-level object representation and analyze the pose of a novel object by comparing the 2D image of the object with the 3D mesh. In this way, the category-level generalization ability of the model could be learned from thousands of annotated images. Based on the category-level repre-

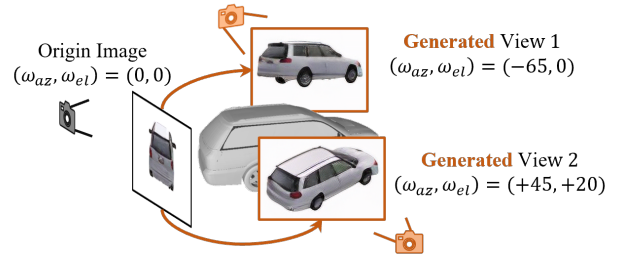


Figure 1: We propose to learn a category-level object pose estimator from the multiple views of the objects in the category. As shown in the figure, by leveraging the generative diffusion model, we generate novel views of an object with controlled poses  $(\omega_{az}, \omega_{el})$  and learn the pose estimator from the multiple views of the objects in the category and their controlled poses.

sation, previous works devote efforts to shape prior [Wang *et al.*, 2024], occlusion problem [Ma *et al.*, 2022] and key-point detection [Tulsiani and Malik, 2015] to learn a more robust category-level pose estimator.

However, these category-level pose estimation methods need hundreds of annotated images for a novel object class to learn a unified representation. Although some researchers [Wang *et al.*, 2021b; Yin *et al.*, 2022] proposed to learn object pose estimators with fewer annotated images, those approaches still require a certain amount of human labor on annotation, which impedes the pathway to millions of object categories in the real world. A natural question is raised: can we learn a category-level object pose estimator without pose annotations?

In this paper, we propose an affirmative answer to this question. Instead of using annotated images to build category-level representations, we learn our object pose estimator from image sets that each image set is generated from a single unannotated image using diffusion models. Built on top of the recent series of diffusion-based 3D generative models [Liu *et al.*, 2023b; Shi *et al.*, 2023], which show the ability to recover the 3D geometry from a single image with viewing controls, we generate the set of images under a controlled pose different from the set of original unannotated images for training. However, we find that the generated images have some artifacts for the image quality, *e.g.*, incorrect texture, and the pose control is rather crude, *i.e.*, noise for the pseudo

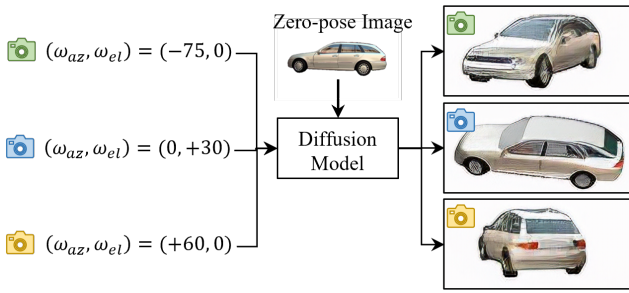


Figure 2: Posed image generation. Given an image containing an object and the pose of a target view  $(\omega_{az}, \omega_{el})$ , we control the diffusion model to generate the target view of the object by leveraging the view pose.

pose label of the generated images. To resolve this, we introduce an image encoder as an information filter for removing unreasonable object details, and a merging strategy that distillates the learned pose discriminability from all learned object representations.

As shown in Figure 1, given a set of object images with target view poses, we first exploit a generative diffusion model (*i.e.*, Zero-1-to-3 [Liu *et al.*, 2023b]) to generate a set of images in a certain pose difference of the object in the original image. We introduce an image encoder for filtering inconsistent details and extracting the feature maps of the generated images. Then we build a separate neural mesh for each instance and jointly optimize all the neural meshes with the image feature maps. The experiments conducted on the PASCAL3D+ [Xiang *et al.*, 2014] and KITTI [Geiger *et al.*, 2013] datasets demonstrate that our approach is capable of performing object pose estimation using a single shot annotation as the definition of pose. Moreover, we compare our approach with the state-of-the-art methods for the few-shot category-level 3D object pose estimation on the PASCAL3D+ dataset. The experimental results demonstrate that our model outperforms previous state-of-the-art methods by a large margin.

In summary, our contribution includes:

- We propose a category-level object pose estimation pipeline that learns 3D object poses without requiring the need for pose annotations.
- We introduce a diffusion-based image generation pipeline, which creates pose-controlled images from a single unannotated image.
- We propose a learning pipeline, which learns object-pose discriminability from multiple generated image sets jointly and combines all the learned instance-specific estimators.
- Experimental results show that our model could predict object poses in a new category by training with unannotated images and achieves state-of-the-art performance on the few-shot pose estimation setting.

## 2 Related Work

**Learning a pose estimator with full supervision.** 3D object pose estimation is a challenging task. Early works either considered the pose estimation challenge as a regression

problem [Tulsiani and Malik, 2015; Mousavian *et al.*, 2017], or studied the problem as a two-step approach *i.e.*, keypoint detection and Perspective-n-Point solving process [Lepetit *et al.*, 2009; Pavlakos *et al.*, 2017; Zhou *et al.*, 2018]. Recently a series of works tried to solve the problem by following the Analysis-by-Synthesis philosophy [Wang *et al.*, 2019; Yen-Chen *et al.*, 2021]. Specifically, they used a differentiable renderer to render a synthesized image and conduct pose estimation by minimizing the reconstruction loss between the synthesized image and the target image. Such "render-and-compare" pipeline has been extended by NeMo [Wang *et al.*, 2021a], in which the comparison is conducted between the extracted feature banks of the synthesized image and target image. However, these approaches need a huge amount of pose annotations, which are time-consuming and laborious for human labeling. In this study, we tried to learn the pose estimator without pose annotations.

**Learning a pose estimator in the few-shot setting.** To reduce the consumption of annotated data, recent studies focused on the pose estimation problem in a few-shot setting [Wang *et al.*, 2021b; Yin *et al.*, 2022; Wang *et al.*, 2022; Jesslen *et al.*, 2023; Yang *et al.*, 2024]. For example, NVSM [Wang *et al.*, 2021b] proposed to learn an object pose estimator with few annotated images and a collection of unlabeled data. FisherMatch [Yin *et al.*, 2022] proposed a teacher-student framework that facilitates the information flow from annotated data to unlabeled data. Although these methods successfully reduce the need for annotated data by training with hundreds of unannotated images, they still require a certain amount of annotated data for each object category, which significantly limits its further applications in the real world when encountering billions of objects in millions of categories. In this study, we try to train the estimator without the need for any pose annotations.

**3D object generation.** Recently, the diffusion models [Ho *et al.*, 2020; Song *et al.*, 2020] bring a storm on the generation tasks [Poole *et al.*, 2022; Liu *et al.*, 2023b; Shi *et al.*, 2023; Lin *et al.*, 2023; Liu *et al.*, 2023a]. The images generated from these models contribute to many downstream applications such as text-to-image generation [Ruiz *et al.*, 2023; Gao *et al.*, 2024], image editing [Kawar *et al.*, 2023] and image style transformation [Zhang *et al.*, 2023]. The high quality of 2D-generated images facilitates many researchers to study the 3D object generation. Zero-1-to-3 [Liu *et al.*, 2023b] is a representative one that exploits an object image to generate the 3D reconstruction of the object. It uses rotation angles to control the generated view of the object. Although its following works such as Zero-1-to-3++ [Shi *et al.*, 2023] improve the image generation quality, the generated views of objects still encounter the image quality issues and inaccurate poses of the generated objects, which hinder the further applications to the real world. In this paper, we leverage the power of the generative diffusion model and propose to learn from the encoded features of the generative view images to reduce the negative impacts.

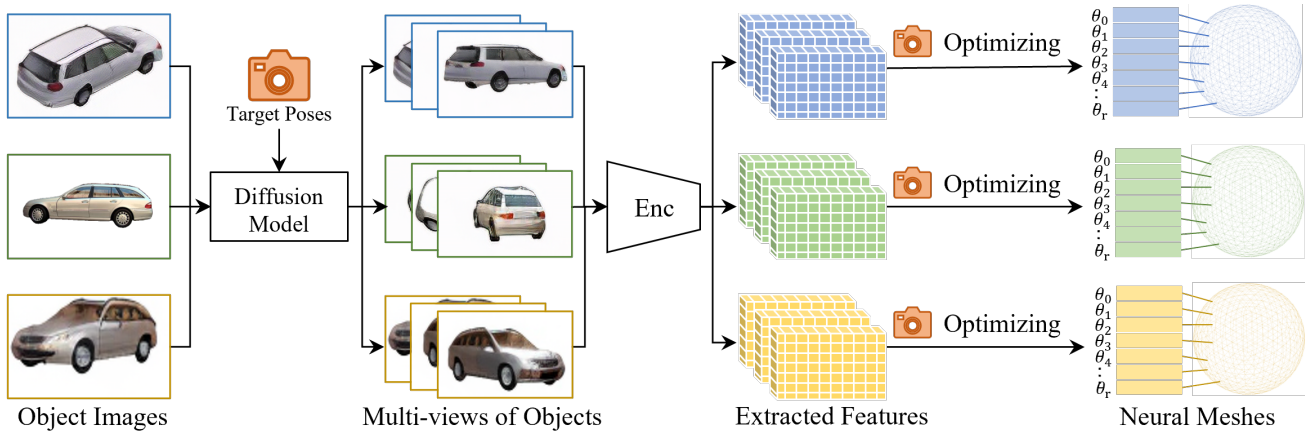


Figure 3: The training pipeline of our model. Given a set of object images, we define the object poses on these images as zero-poses (*i.e.*,  $(\omega_{az}, \omega_{el}) = (0, 0)$ ). Then given the target view poses, we exploit the generative diffusion model to generate the target views of the objects. We introduce an image encoder to extract the image feature maps of these view images. We exploit the image feature maps with the corresponding target poses to optimize the neural mesh for each object.

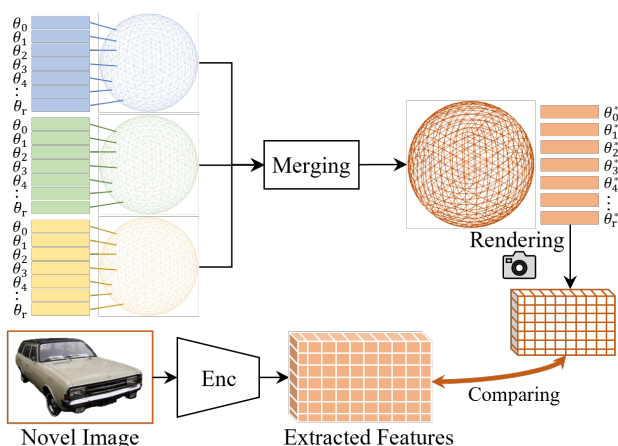


Figure 4: Neural mesh merging strategy and evaluation pipeline. After training, we estimate the relative pose between two meshes and merge two neural meshes with the estimated pose. In the evaluation, We consider the pose of a novel image as a learnable matrix. We render the feature map from the merged neural mesh with the learnable pose and optimize the pose by comparing the rendered feature map with the extracted feature map of the novel image.

### 3 Method

In this section, we introduce our method for learning a category-level object pose estimator without pose annotations. Specifically, given a set of unannotated images  $\mathcal{I}$ , for each image  $I_y \in \mathcal{I}$ , we first define its canonical pose space center at  $P_y$ , where  $P_y$  is unknown during training. In Section 3.1 we introduce how to generate a novel view of an object image under a certain rotation  $\Delta P_m$ . Then we introduce the learning strategy by leveraging the generated views of one object image in Section 3.2. and describe the overall training strategy in Section 3.3. We finally present the evaluation pipeline in Section 3.4.

#### 3.1 Posed Image Generation from Diffusion

As Figure 3 shows, we learn our category-level object pose estimator from the image sets generated by the diffusion model. Each image set  $\mathcal{I}_y = \{I_m \in \mathbb{R}^{H \times W \times 3}\}$  is generated from a real image  $\hat{I}_y$  in the training set. Specifically, we first exploit a segmentation method (*i.e.*, SAM [Kirillov *et al.*, 2023]) to delineate the object from the image. For each delineated object image, we define its canonical pose space center  $P_y \in \mathbb{R}^{3 \times 3}$  as the object pose on the image. Since we do not know the pose of the object, we initialize  $P_y$  as an identity matrix. Then as shown in Figure 2, given the rotation angle  $(\omega_{az}, \omega_{el})$  of a target view, we use a generative diffusion model (*i.e.*, Zero-1-to-3), to generate the object image viewing from the target direction,

$$I_m = \Psi_{gen}(\hat{I}_y, (\omega_{az}, \omega_{el})), \quad (1)$$

where  $I_m$  is the generated object image. By assuming the object facing toward the viewing direction of the camera coordinate of the image, each pose of the generated image can be described as a composition of canonical pose  $P_y$  with an additional rotation  $\Delta P_m$ . The  $\Delta P_m$  is computed by

$$\Delta P_m = T(\omega_{az}, \omega_{el}), \quad (2)$$

where the  $T$  denotes a transformation function (known as the LookAt transformation). Then the rotated object pose of  $I_m$  could be defined by the following equation,

$$P_m = P_y \Delta P_m. \quad (3)$$

Summarily, we obtain an image set  $\mathcal{I}_y$  of the object on the image  $I_y$  containing the generated object images from different angles and the pose set  $\mathcal{P}_y$  containing the corresponding image poses. Due to the limited resolution of the generated image, we exploit the super-resolution model [Wang *et al.*, 2018] to upsample the image from  $256 \times 256$  to  $512 \times 512$ .

#### 3.2 Canonical Specific Object Pose Learning

We formulate our object pose estimator following Neural Meshes Models [Wang *et al.*, 2021a]. Specifically, for the

image set  $\mathcal{I}_y$ , we learn a neural mesh  $\mathfrak{N}_y = \{\mathcal{V}_y, \mathcal{A}_y, \Theta_y\}$ , which consists a set of mesh vertices  $\mathcal{V}_y = \{V_k \in \mathbb{R}^3\}_{k=1}^{K_y}$ , triangular faces  $\mathcal{A}_y = \{A_k \in \mathbb{N}^3\}_{k=1}^{K'_y}$  and feature vectors on each vertex  $\Theta_y = \{\theta_k \in \mathbb{R}^d\}_{k=1}^{K_y}$ , where  $K_y$  and  $K'_y$  are the numbers of vertices and faces of each mesh. Different from the uniformly sampled or cuboid object meshes used in NeMo [Wang et al., 2021a], we exploit the geodesic polyhedrons as the object geometry representations, which allow to learn the neural meshes without the assumption of the canonical pose of each instance, since the geometry of geodesic polyhedrons is independent of the pose.

In the training, we first use a ResNet feature extractor [He et al., 2016] to extract the feature map  $\Phi_w(I_m) = F \in \mathbb{R}^{c \times h \times w}$  from the input image  $I_m \in \mathcal{I}_y$ , where  $\Phi_w$  is the feature extractor with network parameters  $w$ . Then, to learn the vertex features  $\theta_k$ , as well as the feature extractor  $\Phi_w$ , we calculate the world-to-screen transformation  $\Omega_m$  given a camera pose  $P_m \in \mathbb{R}^3$ . To find the vertex  $k$  corresponding feature  $f_k = F(p_k)$  at pixel  $p_k$  on the feature map, we compute the projected location of each vertex on the feature map  $p_k = \Omega_m(V_k)$ . Besides, the visibility  $o_k$  is determined for each vertex in the image, *i.e.*,  $o_k = 1$  if vertex  $k$  is visible, and vice versa. Specifically, we render the depth map  $\mathbf{D} = \text{Render}(\mathfrak{N}_y, \Omega_m)$  and compute the vertex-to-camera distance  $\mathbf{d}_k = \|\mathbf{Q} - V_k\|_2$ . Then the vertex visibility is computed as

$$o_k = \begin{cases} 0, & \|\mathbf{D}_{p_k} - \mathbf{d}_k\|_2 > \tau_r \\ 1, & \|\mathbf{D}_{p_k} - \mathbf{d}_k\|_2 \leq \tau_r \end{cases}, \quad (4)$$

where  $\tau_r$  is a preset threshold. We learn the vertex features  $\theta_k$  using the momentum update strategy [Bai et al., 2023],

$$\theta_k \leftarrow o_k(1 - \beta) \cdot f_k + (1 - o_k + \beta \cdot o_k)\theta_k, \quad (5)$$

where  $\beta$  is the momentum for the update process.

Our learning optimal of the feature extractor is to enlarge the feature distance  $\|\theta_j - f_i\|_2$  if  $\|V_i - V_j\|_2$  is above a desired threshold. Such properties of features allow us to use differentiable rendering to find the optimal alignment of the vertices on the 3D model and corresponding locations on the 2D image. To achieve this, we use the contrastive loss [Bai et al., 2023] to learn the weights  $w$ :

$$\mathcal{L}_m^{fg} = - \sum_k o_k \cdot \log\left(\frac{e^{\kappa f_k \cdot \theta_k}}{\sum_{\theta_l \in \mathcal{Y}_y, v_l \notin \mathcal{N}_k} e^{\kappa f_k \cdot \theta_l}}\right), \quad (6)$$

where  $\kappa$  is a preset softmax temperature, and  $\mathcal{N}_k$  indicates a spacial neighborhood of  $V_k$ , which controls specially accuracy of the learned features. We also include the background loss  $L_y^{bg}$  following [Bai et al., 2023]. During training, we jointly optimize all the neural meshes  $\{\mathfrak{N}_1, \mathfrak{N}_2, \dots, \mathfrak{N}_Y\}$  where  $Y$  is the number of image instances.

### 3.3 Training Strategy

**Optimization loss.** As we describe how to optimize a neural mesh with an input image in Section 3.2, now we introduce how to train the image encoder by jointly optimizing multiple neural meshes. For the generated images  $\mathcal{I}_m$ , we

compute the feature loss  $\mathcal{L}_m$  by exploiting (6). The final loss could be formulated as

$$\mathcal{L}_{\text{train}} = \sum_{\mathcal{I}_y \in \mathfrak{S}} \mathcal{L}_y^{\text{train}} = \sum_{\mathcal{I}_y \in \mathfrak{S}} \sum_{I_m \in \mathcal{I}_y} (\mathcal{L}_m^{fg} + \mathcal{L}_m^{bg}). \quad (7)$$

**Instance Neural Mesh merging via canonicalization.** We suppose that during training, each neural mesh learns a specific representation related to the corresponding object. Hence we propose a mechanism to merge the well-trained meshes into one category-level object representation. As shown Figure 4, although we do not know the relative ground truth poses between different meshes, we could estimate the relative poses by exploiting the learned feature vectors. Specifically, given two neural meshes  $\mathfrak{N}_i = \{\mathcal{V}_i, \mathcal{A}_i, \Theta_i\}$ ,  $\mathfrak{N}_j = \{\mathcal{V}_j, \mathcal{A}_j, \Theta_j\}$ , we define that the mesh  $\mathfrak{N}_j$  is the anchor mesh that we always try to merge other meshes into the mesh  $\mathfrak{N}_j$ . We further define a rotation matrix  $R$  that rotates the neural mesh  $\mathfrak{N}_i$  at the target angle. Then we could calculate the vertex distance between the vertex  $V_m$  in  $\mathcal{V}_j$  from mesh  $\mathfrak{N}_j$  and the rotated vertex from the mesh  $\mathfrak{N}_i$ .

$$D_{mn}^{\text{vertex}}(R) = |V_m - RV_n|, \quad (8)$$

where  $V_n \in \mathcal{V}_i$  is a vertex of the neural mesh  $\mathfrak{N}_i$ . The corresponding feature distance of two vertices could be calculated by using the vertex distance  $D_{mn}^{\text{vertex}}(R)$ ,

$$D_m^{\text{feat}}(R) = \theta_m - \sum_{V_k \in \mathcal{V}_n} \left(\frac{\theta_k}{D_{mn}^{\text{vertex}}(R)}\right), \quad (9)$$

where  $D_m^{\text{feat}}(R)$  is the corresponding feature distance of two vertices under the rotation  $R$ .  $\theta_m \in \Theta_j$  is the feature vector of  $V_j$  and  $\theta_n \in \Theta_i$  is the feature vector of  $V_i$ . Hence the optimal  $R^*$  could be found by minimizing the following equation,

$$R^* = \arg \min_R \sum_{\theta_m \in \Theta_j} D_m^{\text{feat}}(R). \quad (10)$$

Then we exploit the optimal  $R^*$  to calculate the feature distance  $D_m^{\text{feat}}(R^*)$  between two meshes and merge two meshes when the distance  $D_m^{\text{feat}}(R^*) < \tau_{\text{merge}}$ .  $\tau_{\text{merge}}$  is the merging threshold and we set  $\tau_{\text{merge}}$  to 0.8 in this study. The feature vector of each vertex  $\theta_m^* \in \Theta^*$  after merging could be calculated by the following equation,

$$\theta_m^* = \frac{1}{2} \left( \theta_m + \sum_{V_k \in \mathcal{V}_n} \left(\frac{\theta_k}{D_{mn}^{\text{vertex}}(R^*)}\right) \right). \quad (11)$$

We also exploit the image set  $\mathcal{I}_i$  that is used to train the mesh  $\mathfrak{N}_i$  to train the anchor mesh  $\mathfrak{N}_j$ . Specifically, let  $P_n$  denote the image pose  $I_n \in \mathcal{I}_i$ , we train the anchor mesh  $\mathfrak{N}_j$  with the image  $I_n$  and the corresponding new pose  $P'_n$ ,

$$P'_n = P_n R^*. \quad (12)$$

During training, we randomly select an anchor mesh and merge the neural meshes by exploiting the above strategy and obtain the category-level feature vectors  $\Theta^*$ .

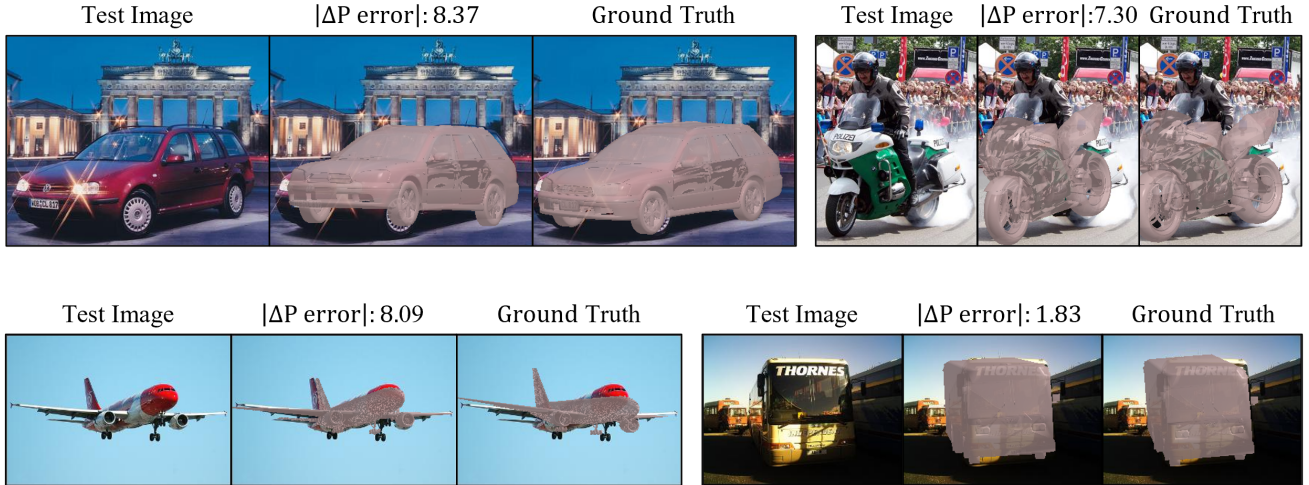


Figure 5: Qualitative results of training the pose estimator without pose annotations. We present four cases on the car, motorbike, aeroplane and bus categories, respectively. We use the CAD model of each category for better visualization and present the pose estimation errors on the top of the prediction images. Without requiring any pose annotations, our model still successfully predicts object poses in low pose estimation errors.

Method	1		7		20		50	
	Med. ↓	Acc <sub>30</sub> ↑	Med. ↓	Acc <sub>30</sub> ↑	Med. ↓	Acc <sub>30</sub> ↑	Med. ↓	Acc <sub>30</sub> ↑
Res50-Generic	—	—	39.1	36.1	26.3	45.2	20.2	54.6
Res50-Specific	—	—	46.5	29.6	29.4	42.8	23.0	50.4
StarMap [Zhou et al., 2018]	—	—	49.6	30.7	46.4	35.6	27.9	53.8
NeMo [Wang et al., 2021a]	—	—	60.0	38.4	33.3	51.7	22.1	69.3
NVSM [Wang et al., 2021b]	—	—	37.5	53.8	28.7	61.7	24.2	65.6
FisherMatch [Yin et al., 2022]	—	—	28.3	56.8	23.8	63.6	16.1	75.7
Ours	<b>29.3</b>	<b>58.8</b>	<b>26.3</b>	<b>60.7</b>	<b>22.8</b>	<b>69.1</b>	<b>15.4</b>	<b>77.4</b>
Full Supervision [Wang et al., 2021a]	8.1	89.6	8.1	89.6	8.1	89.6	8.1	89.6

Table 1: Few-shot pose estimation results on the PASCAL3D+ dataset. We indicate the number of annotations during training for each category and evaluate all the approaches using Accuracy (in percent, higher better) and Median Error (in degree, lower better). Notably, "1 instance" denotes that we train our model without annotations and only exploit one pose annotation on an image as the pose definition on the evaluation set. We also present the results from the fully supervised model at the bottom line. It can be seen that our model outperforms other state-of-the-art methods in the few-shot settings. Moreover, even without annotation images in the training steps, the Acc<sub>30</sub> performance of our model is still better than other methods that need seven annotated images for training.

### 3.4 Evaluation

As shown in Figure 4, after training, we exploit the feature extractor  $\Phi_w(I_m)$  and the anchor neural mesh with the merged feature vectors  $\Theta^*$  for estimating the 3D object pose on a novel image. We follow previous works [Wang et al., 2021a; Wang et al., 2021b] and implement 3D pose estimation in a render-and-compare manner. Specifically, given a test image  $I_{test}$ , we extract its feature maps by using the feature extractor  $F_{test} = \Phi(I_{test})$ . At the same time, we initialize the 3D pose prediction  $P$  by sampling a set of preset initial pose. Then we optimize the 3D pose  $P$  by exploiting a differentiable renderer  $\mathfrak{R}$  to synthesize feature maps  $F_{syn} = \mathfrak{R}(\mathfrak{N}, P)$  and computing a feature reconstruction loss between  $F_{syn}$  and  $F_{test}$ . We conduct the gradient optimization of  $P$  iteratively. Once the optimization is done, we record the optimized  $P$  as the final pose of the test image.

Method	1		7	
	Med. ↓	Acc <sub>10</sub> ↑	Med. ↓	Acc <sub>10</sub> ↑
NeMo [Wang et al., 2021a]	—	—	73.63	11.76
NVSM [Wang et al., 2021b]	—	—	22.07	21.18
Ours	<b>69.43</b>	<b>25.54</b>	<b>16.52</b>	<b>36.42</b>

Table 2: Quantitative results on the car category from the KITTI dataset. While other methods need seven annotated images to train, our model outperforms these methods in the Acc<sub>10</sub> index without any annotations in the training step.

## 4 Experiment

In this section, we discuss our experimental results. We first present a brief introduction of our experiment setup. Then we discuss the pose estimation results by training with few pose annotations and without pose annotations. In the end,

N. Obj	car			bus		
	Med. ↓	Acc <sub>10</sub> ↑	Acc <sub>30</sub> ↑	Med. ↓	Acc <sub>10</sub> ↑	Acc <sub>30</sub> ↑
1	92.32	7.0	28.2	17.69	32.7	69.7
20	33.28	7.5	44.6	9.10	42.9	86.3
50	20.23	17.6	65.0	7.62	68.0	85.7
100	13.47	32.4	70.4	<b>7.43</b>	72.0	86.8
150	<b>11.26</b>	<b>43.6</b>	<b>71.7</b>	7.50	<b>72.2</b>	<b>87.0</b>

Table 3: Ablation study on the number of the training objects in the unannotated images. We present the performance of car and bus categories in the PASCAL3D+ dataset. By leveraging multiple views of more objects in the unannotated images, our model learns stronger generalization ability on the category-level pose estimation tasks and reaches better performance on the accuracy and median error indices.

we conduct a series of ablation studies.

#### 4.1 Experiment Setup

**Dataset.** We evaluated our model on the PASCAL3D+ dataset [Xiang *et al.*, 2014] and KITTI dataset [Geiger *et al.*, 2013]. For the PASCAL3D+ dataset, we followed previous works [Wang *et al.*, 2020; Wang *et al.*, 2021b; Yin *et al.*, 2022] to evaluate the performance on six categories: aeroplane, bicycle, boat, bus, car and motorbike. The images in these categories have a relatively evenly distributed pose regarding the azimuth angle. For the KITTI dataset, we followed previous works [Wang *et al.*, 2021b] to evaluate the performance on the car category. We cropped the images with the bounding boxes in the datasets to ensure that the objects are located in the center of the images. We also followed the official KITTI protocol to split the dataset into a training set including 2047 images and a testing set including 681 images.

**Implementation details.** We used ResNet50 [He *et al.*, 2016] pretrained on ImageNet [Deng *et al.*, 2009] as the image encoder. We evenly sampled  $\omega_{az}$  and  $\omega_{el}$  at the fixed 15-degree distance from -90 to 90 degrees. We generated the multiple views of the objects in the training images by using Zero-1-to-3 [Liu *et al.*, 2023b]. As the generated images from Zero-1-to-3 have similar scales, we manually adjust a unified camera distance for all the generated images. Please refer to *supplementary material* for more implementation details.

**Evaluation.** The 3D object pose estimation task predicts three rotation parameters: azimuth, elevation, and in-plane rotation. We follow previous works [Wang *et al.*, 2021a; Wang *et al.*, 2021b; Yin *et al.*, 2022] and suppose the object scale and center are known. We calculate the pose estimation error between the predicted rotation matrix and the ground truth:  $\Delta(P_{pred}, P_{gt}) = \frac{\| \log m(P_{pred}^T P_{gt}) \|_F}{\sqrt{2}}$ . We report accuracy on two thresholds  $\frac{\pi}{6}$  (ACC<sub>30</sub>) and  $\frac{\pi}{18}$  (ACC<sub>10</sub>) and the median error (Med.) of the prediction.

#### 4.2 Training with Few Pose Annotations

As previous works [Wang *et al.*, 2021b; Yin *et al.*, 2022] only trained the category-level pose estimator in the few-shot settings, in this section we tested the performance of our model by training with few annotated images for a fair comparison.

N. View	car			motorbike		
	Med. ↓	Acc <sub>10</sub> ↑	Acc <sub>30</sub> ↑	Med. ↓	Acc <sub>10</sub> ↑	Acc <sub>30</sub> ↑
1	52.13	4.3	24.4	70.53	8.2	26.8
5	25.81	6.2	59.5	47.67	11.6	37.7
10	13.75	30.3	66.9	31.29	11.1	49.0
20	<b>12.36</b>	<b>38.3</b>	<b>67.9</b>	<b>23.77</b>	<b>15.5</b>	<b>56.9</b>

Table 4: Ablation study on the number of training views of each object. We report the pose estimation results on the car and motorbike categories in the PASCAL3D+ dataset. Our model benefits from more object views to learn a better pose correspondence and hence achieve better results on the median error and accuracy indices.

Specifically, we exploited the annotated images to train the anchor neural mesh described in Section 3.3 while jointly optimizing other neural meshes with unannotated images. We reported the pose estimation results on the PASCAL3D+ and KITTI datasets.

**Results on the PASCAL3D+ dataset.** For each object category, we follow previous works [Wang *et al.*, 2021b; Yin *et al.*, 2022] to train our model with 7, 20 and 50 object images with annotated poses. We also list the performances of a series of state-of-the-art methods [Wang *et al.*, 2021a; Wang *et al.*, 2021b; Yin *et al.*, 2022; He *et al.*, 2016; Zhou *et al.*, 2018] in Table 1. We evaluated StarMap [Zhou *et al.*, 2018], NeMo [Wang *et al.*, 2021a] and FisherMatch [Yin *et al.*, 2022] as our baselines as they are recently proposed approaches for few-shot 3D pose estimation. We also implemented a baseline that considers the object pose estimation problem as a classification task as mentioned in StarMap [Zhou *et al.*, 2018]. Concretely, we implemented a category-specific (Res50-Specific) classifier and a non-specific (Res50-Generic) classifier. The former formulates the object pose estimation problem for all categories as one single classification task and the latter learns a classifier for each category. Table 1 shows that our proposed approach achieves great improvement compared to other state-of-the-art methods.

**Results on the KITTI Dataset.** Table 2 presents the pose estimation results on the KITTI dataset. We compare our model with NeMo [Wang *et al.*, 2021a] and NVSM [Wang *et al.*, 2021b] since they are two of the most competitive methods in this setting. In addition, since the keypoint annotations are not provided in the KITTI dataset, StarMap [Zhou *et al.*, 2018] cannot be trained on the KITTI dataset without the annotations. Table 2 shows that our method outperforms other state-of-the-art methods by a large margin. It demonstrates that our model learns a strong object pose estimator from few annotated images.

#### 4.3 Training without Pose Annotations

In this section, we conduct a series of experiments of training an object pose estimator without pose annotations. Specifically, for each category, we trained our model by using multiple views of objects and predicted object poses on the evaluation dataset with the pre-trained model. To evaluate the performance, we exploited one image with the annotated pose

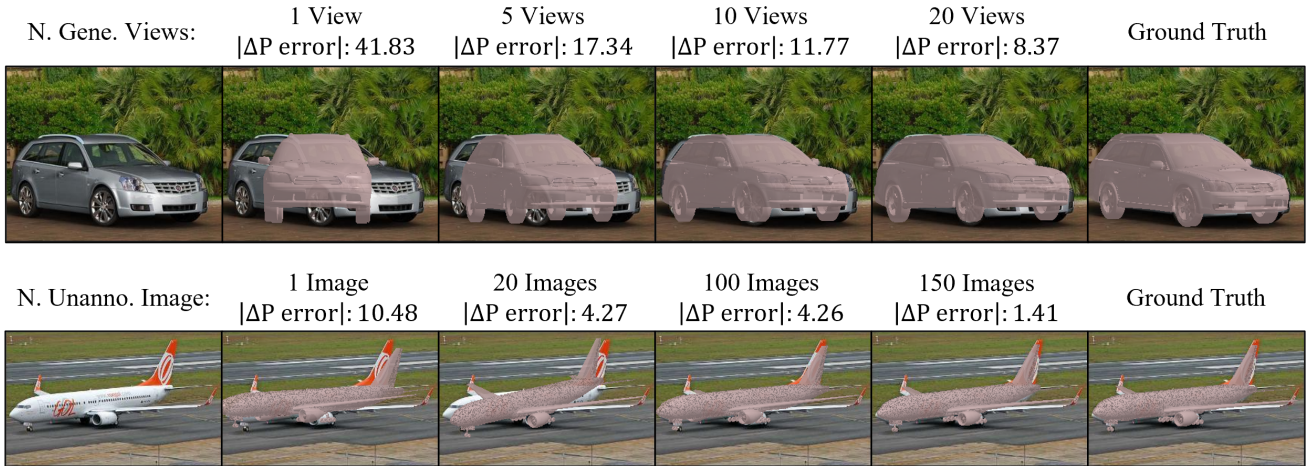


Figure 6: Ablation study on the number of generated views (**top**) and unannotated images (**bottom**). We present the results with the corresponding CAD models for better visualization. Our model learns stronger pose correspondence by increasing the object views generated by the diffusion model. Moreover, our model could learn stronger generalization ability by training with more objects from unannotated images.

to make an alignment of coordinate systems between the predicted poses and the ground truth poses. It is worth noting that previous works [Wang *et al.*, 2021a; Wang *et al.*, 2021b; Deng *et al.*, 2009; Yin *et al.*, 2022] fail to predict poses due to the lack of annotated data. We tested the performance of our model on the PASCAL3D+ dataset in Table 1 and the KITTI dataset in Table 2.

**Performance on the PASCAL3D+ dataset.** We present the visualization results on Figure 5. In Table 1, even without any pose annotations for training, our model achieves 29.3 on median error, which is comparable with the state-of-the-art performance on the few-shot setting with 7 annotated poses. Moreover, our model could reach 58.8% performance on the  $\text{Acc}_{30}$  matrix, which significantly outperforms other state-of-the-art methods on the seven-annotated setting. Both Figure 5 and Table 1 demonstrate that our model could learn a strong 3D object pose correspondence from multiple views of objects.

**Performance on the KITTI dataset.** In Table 2, we present the performance of our model by training without any annotations on the KITTI dataset. Our model achieves 69.43 performance on the median error and 25.54 on  $\text{Acc}_{10}$ . Since the KITTI dataset contains the street scene in the autonomous driving setting, the cropped car images are smaller than the ones on the PASCAL3D+ dataset. In this way, the image quality of the novel object view generated from the Zero-1-to-3 [Liu *et al.*, 2023b] is much lower than the one in the PASCAL3D+ dataset, which leads to a higher median error index. However, even without the object poses, our method reaches significantly better performance than the state-of-the-art methods on the seven-shot setting. It demonstrates the effectiveness of our model by learning a strong 3D pose correspondence from multiple object views.

#### 4.4 Ablation studies

In this section, we conduct a series of ablation studies of our model by training our model without pose annotations. We

first test the performance of our model with different numbers of unannotated images in the training pipeline. Then we conduct the ablation study on the number of object views.

**Number of the unannotated images.** Since our model exploits multiple neural meshes for training with multiple views of the objects in the unannotated images, we test the model performance by using different numbers of unannotated images. We present the results in Figure 6 and Table 3. When training our model only with one neural mesh and the multiple views from one object image, Figure 6 shows that the predicted pose has a relatively large pose error and the performance of  $\text{Acc}_{10}$  and  $\text{Acc}_{30}$  on the car and bus categories in the PASCAL3D+ dataset has a significant drop, which demonstrates that the category-level generalization ability can hardly be learned from only one object in the category. With the increase of unannotated images, the performance of  $\text{Acc}_{10}$  and  $\text{Acc}_{30}$  indices gradually increase, which demonstrates that the category-level generalization ability of our model could be obtained by jointly learning from multiple views of hundreds of objects in the unannotated images.

**Number of the object views.** As different views of an object provide different details of 3D pose correspondence, we evaluate the correspondence learning ability by training with different numbers of object views. In Table 4 and Figure 6, we present the results on the PASCAL3D+ dataset. Since the 3D pose correspondence cannot learn from one view of an object, there is a performance drop when training the model with only one view of each object. By increasing the training views of objects, our model gradually reaches higher performances on  $\text{Acc}_{10}$  and  $\text{Acc}_{30}$  indices and has lower median errors of pose estimation. It shows that the multiple object views significantly contribute to the pose estimator learning.

## 5 Conclusion

In this paper, we propose to learn an object pose estimator without pose annotations. By leveraging the diffusion model

*i.e.*, Zero-1-to-3 to generate multiple views of objects, we propose to learn the pose estimator from the generated view images. As the generated images from the diffusion model have both image quality issues and severe noise on the pose labels, we propose to exploit an image encoder to extract the image features of different image views and learn the pose correspondence from the extracted image features. Experiments on the PASCAL3D+ and KITTI datasets demonstrate the effectiveness of our model.

**Acknowledgments.** We gratefully acknowledge support via Army Research Laboratory award W911NF2320008 and ONR with award N00014-21-1-2812.

## References

- [Bai *et al.*, 2023] Yutong Bai, Angtian Wang, Adam Kortylewski, and Alan Yuille. Coke: Localized contrastive learning for robust keypoint detection. In *WACV*, 2023.
- [Deng *et al.*, 2009] Jia Deng, Wei Dong, Richard Socher, Li-Jia Li, Kai Li, and Li Fei-Fei. ImageNet: A large-scale hierarchical image database. In *CVPR*, pages 248–255, 2009.
- [Gao *et al.*, 2024] Xuehao Gao, Yang Yang, Zhenyu Xie, Shaoyi Du, Zhongqian Sun, and Yang Wu. GUESS: Gradually enriching synthesis for text-driven human motion generation. *IEEE TVCG*, 2024.
- [Geiger *et al.*, 2013] Andreas Geiger, Philip Lenz, Christoph Stiller, and Raquel Urtasun. Vision meets robotics: The kitti dataset. *The International Journal of Robotics Research*, 32(11):1231–1237, 2013.
- [He *et al.*, 2016] Kaiming He, Xiangyu Zhang, Shaoqing Ren, and Jian Sun. Deep residual learning for image recognition. In *CVPR*, pages 770–778, 2016.
- [Ho *et al.*, 2020] Jonathan Ho, Ajay Jain, and Pieter Abbeel. Denoising diffusion probabilistic models. In *NeurIPS*, volume 33, pages 6840–6851, 2020.
- [Jesslen *et al.*, 2023] Artur Jesslen, Guofeng Zhang, Angtian Wang, Alan Yuille, and Adam Kortylewski. Robust 3d-aware object classification via discriminative render-and-compare. *arXiv preprint arXiv:2305.14668*, 2023.
- [Kawar *et al.*, 2023] Bahjat Kawar, Shiran Zada, Oran Lang, Omer Tov, Huiwen Chang, Tali Dekel, Inbar Mosseri, and Michal Irani. Imagic: Text-based real image editing with diffusion models. In *CVPR*, pages 6007–6017, 2023.
- [Kirillov *et al.*, 2023] Alexander Kirillov, Eric Mintun, Nikhila Ravi, Hanzi Mao, Chloe Rolland, Laura Gustafson, Tete Xiao, Spencer Whitehead, Alexander C. Berg, Wan-Yen Lo, Piotr Dollár, and Ross Girshick. Segment anything. *arXiv:2304.02643*, 2023.
- [Lepetit *et al.*, 2009] Vincent Lepetit, Francesc Moreno-Noguer, and Pascal Fua. Ep-n-p: An accurate o(n) solution to the p-n-p problem. *IJCV*, 81:155–166, 2009.
- [Lin *et al.*, 2023] Chen-Hsuan Lin, Jun Gao, Luming Tang, Towaki Takikawa, Xiaohui Zeng, Xun Huang, Karsten Kreis, Sanja Fidler, Ming-Yu Liu, and Tsung-Yi Lin. Magic3D: High-resolution text-to-3d content creation. In *CVPR*, pages 300–309, 2023.
- [Liu *et al.*, 2023a] Minghua Liu, Chao Xu, Haian Jin, Linghao Chen, Mukund Varma, Zexiang Xu, and Hao Su. One-2-3-45: Any single image to 3d mesh in 45 seconds without per-shape optimization. In *NeurIPS*, 2023.
- [Liu *et al.*, 2023b] Ruoshi Liu, Rundi Wu, Basile Van Hoorick, Pavel Tokmakov, Sergey Zakharov, and Carl Vondrick. Zero-1-to-3: Zero-shot one image to 3d object. In *ICCV*, pages 9298–9309, 2023.
- [Ma *et al.*, 2022] Wufei Ma, Angtian Wang, Alan Yuille, and Adam Kortylewski. Robust category-level 6d pose estimation with coarse-to-fine rendering of neural features. In *ECCV*, pages 492–508, 2022.
- [Mousavian *et al.*, 2017] Arsalan Mousavian, Dragomir Anguelov, John Flynn, and Jana Kosecka. 3d bounding box estimation using deep learning and geometry. In *CVPR*, pages 7074–7082, 2017.
- [Pavlakos *et al.*, 2017] Georgios Pavlakos, Xiaowei Zhou, Aaron Chan, Konstantinos G Derpanis, and Kostas Daniilidis. 6-dof object pose from semantic keypoints. In *ICRA*, pages 2011–2018, 2017.
- [Poole *et al.*, 2022] Ben Poole, Ajay Jain, Jonathan T. Barron, and Ben Mildenhall. DreamFusion: Text-to-3d using 2d diffusion. In *ICLR*, 2022.
- [Ruiz *et al.*, 2023] Nataniel Ruiz, Yuanzhen Li, Varun Jampani, Yael Pritch, Michael Rubinstein, and Kfir Aberman. Dreambooth: Fine tuning text-to-image diffusion models for subject-driven generation. In *CVPR*, pages 22500–22510, 2023.
- [Shi *et al.*, 2023] Ruoxi Shi, Hansheng Chen, Zhuoyang Zhang, Minghua Liu, Chao Xu, Xinyue Wei, Linghao Chen, Chong Zeng, and Hao Su. Zero123++: a single image to consistent multi-view diffusion base model, 2023.
- [Song *et al.*, 2020] Jiaming Song, Chenlin Meng, and Stefano Ermon. Denoising diffusion implicit models. In *ICLR*, 2020.
- [Tulsiani and Malik, 2015] Shubham Tulsiani and Jitendra Malik. Viewpoints and keypoints. In *CVPR*, June 2015.
- [Wang *et al.*, 2018] Xintao Wang, Ke Yu, Shixiang Wu, Jinjin Gu, Yihao Liu, Chao Dong, Yu Qiao, and Chen Change Loy. ESRGAN: Enhanced super-resolution generative adversarial networks. In *ECCV Workshops*, 2018.
- [Wang *et al.*, 2019] He Wang, Srinath Sridhar, Jingwei Huang, Julien Valentin, Shuran Song, and Leonidas J Guibas. Normalized object coordinate space for category-level 6d object pose and size estimation. In *CVPR*, pages 2642–2651, 2019.
- [Wang *et al.*, 2020] Angtian Wang, Yihong Sun, Adam Kortylewski, and Alan L Yuille. Robust object detection under occlusion with context-aware compositionalsnets. In *Proceedings of the IEEE/CVF conference on computer vision and pattern recognition*, pages 12645–12654, 2020.
- [Wang *et al.*, 2021a] Angtian Wang, Adam Kortylewski, and Alan Yuille. NeMo: Neural mesh models of contrastive features for robust 3d pose estimation. In *ICLR*, 2021.



- [Wang *et al.*, 2021b] Angtian Wang, Shenxiao Mei, Alan L Yuille, and Adam Kortylewski. Neural view synthesis and matching for semi-supervised few-shot learning of 3d pose. *NeurIPS*, 34:7207–7219, 2021.
- [Wang *et al.*, 2022] Angtian Wang, Peng Wang, Jian Sun, Adam Kortylewski, and Alan Yuille. Voge: a differentiable volume renderer using gaussian ellipsoids for analysis-by-synthesis. *arXiv preprint arXiv:2205.15401*, 2022.
- [Wang *et al.*, 2024] Angtian Wang, Wufei Ma, Alan Yuille, and Adam Kortylewski. Neural textured deformable meshes for robust analysis-by-synthesis. In *WACV*, pages 3108–3117, 2024.
- [Xiang *et al.*, 2014] Yu Xiang, Roozbeh Mottaghi, and Silvio Savarese. Beyond pascal: A benchmark for 3d object detection in the wild. In *WACV*, pages 75–82, 2014.
- [Yang *et al.*, 2024] Jiahao Yang, Wufei Ma, Angtian Wang, Xiaoding Yuan, Alan Yuille, and Adam Kortylewski. Robust category-level 3d pose estimation from diffusion-enhanced synthetic data. In *Proceedings of the IEEE/CVF Winter Conference on Applications of Computer Vision*, pages 3446–3455, 2024.
- [Yen-Chen *et al.*, 2021] Lin Yen-Chen, Pete Florence, Jonathan T. Barron, Alberto Rodriguez, Phillip Isola, and Tsung-Yi Lin. iNeRF: Inverting neural radiance fields for pose estimation. In *IROS*, 2021.
- [Yin *et al.*, 2022] Yingda Yin, Yingcheng Cai, He Wang, and Baoquan Chen. FisherMatch: Semi-supervised rotation regression via entropy-based filtering. In *CVPR*, pages 11164–11173, 2022.
- [Zhang *et al.*, 2023] Yuxin Zhang, Nisha Huang, Fan Tang, Haibin Huang, Chongyang Ma, Weiming Dong, and Changsheng Xu. Inversion-based style transfer with diffusion models. In *CVPR*, pages 10146–10156, June 2023.
- [Zhou *et al.*, 2018] Xingyi Zhou, Arjun Karapur, Linjie Luo, and Qixing Huang. Starmap for category-agnostic keypoint and viewpoint estimation. In *ECCV*, pages 318–334, 2018.